Supporting Information

for

Ammonia Synthesis from Electrochemical Reduction of Nitrate by Using Boron-doped Diamond Electrodes

Satoru Kuramochi, Andrea Fiorani,* Yasuaki Einaga*

Department of Chemistry, Keio University, 3-14-1 Hiyoshi, Yokohama 223-8522, Japan

Email: andrea.fiorani@keio.jp; einaga@chem.keio.ac.jp

(Contents)

Table of contents

1. Chemicals

Sodium Perchlorate Monohydrate ($NaClO_4•H_2O$, ≥98.0%), Sodium Chloride (NaCl, ≥99.0%), Sodium Nitrate ($NaNO_3$, ≥99.0%), Sodium Hydroxide (NaOH, ≥97.0%), Phosphoric Acid (H_3PO_4, 85.0wt.%, ρ=1.685 g/mL), Sodium Dihydrogenphosphate Dihydrate ($NaH_2PO_4•H_2O$, ≥99.0%), Disodium Hydrogenphosphate (Na_2HPO_4, ≥99.0%), Trisodium Phosphate 12-Water (Na_3PO_4, ≥99.0%), N-1-Naphthylenediaminde Dihydrochloride (≥95.0%), 4-Aminobenzenesulfonamide(≥99.7%), Ammonium Chloride (NH_4Cl, ≥99.5%), Salicylic Acid (HOC_6H_4COOH, ≥99.5%), Trisodium Citrate ($C_6H_5Na_3O_7$, ≥99.0%), Sodium Hypochlorite Pentahydrate ($NaOCl•5H_2O$, 39.0%), Sodium Pentacyanonitrosylferrate(III) Dihydrate ($Na_2Fe(CN)_5NO•2H_2O$, ≥99.0%), Hydrochloric Acid (HCl, 35~39%) were purchased at Fujifilm Wako. Sulfamic Acid (NH_2SO_3H, ≥99.3%) was purchased at Sigma Aldrich. Nitrogen gas (N_2, 99.99995%) was purchased at Taiyo Nippon Sanso JFP. Deionized (DI) water was obtained from a DIRECT-Q UV3 system (Millipore) with a resistivity of 18.2 MΩ·cm at 25 °C.

2. Synthesis and characterization of Boron-doped Diamond (BDD)

BDD was prepared by microwave plasma-assisted chemical vapor deposition (MPCVD, AX5250M, AsTeX corp.) method. Trimethyl borate and acetone mixed at a B/C ratio of 0.1, 0.2, 0.5, 1% were used and boron and carbon source, respectively. The formation of BDD was confirmed by SEM and Raman spectrum measurements.

The diamond is polycrystalline exhibiting polygonal crystals, characteristic of (111) facet, and triangular (100) facet.

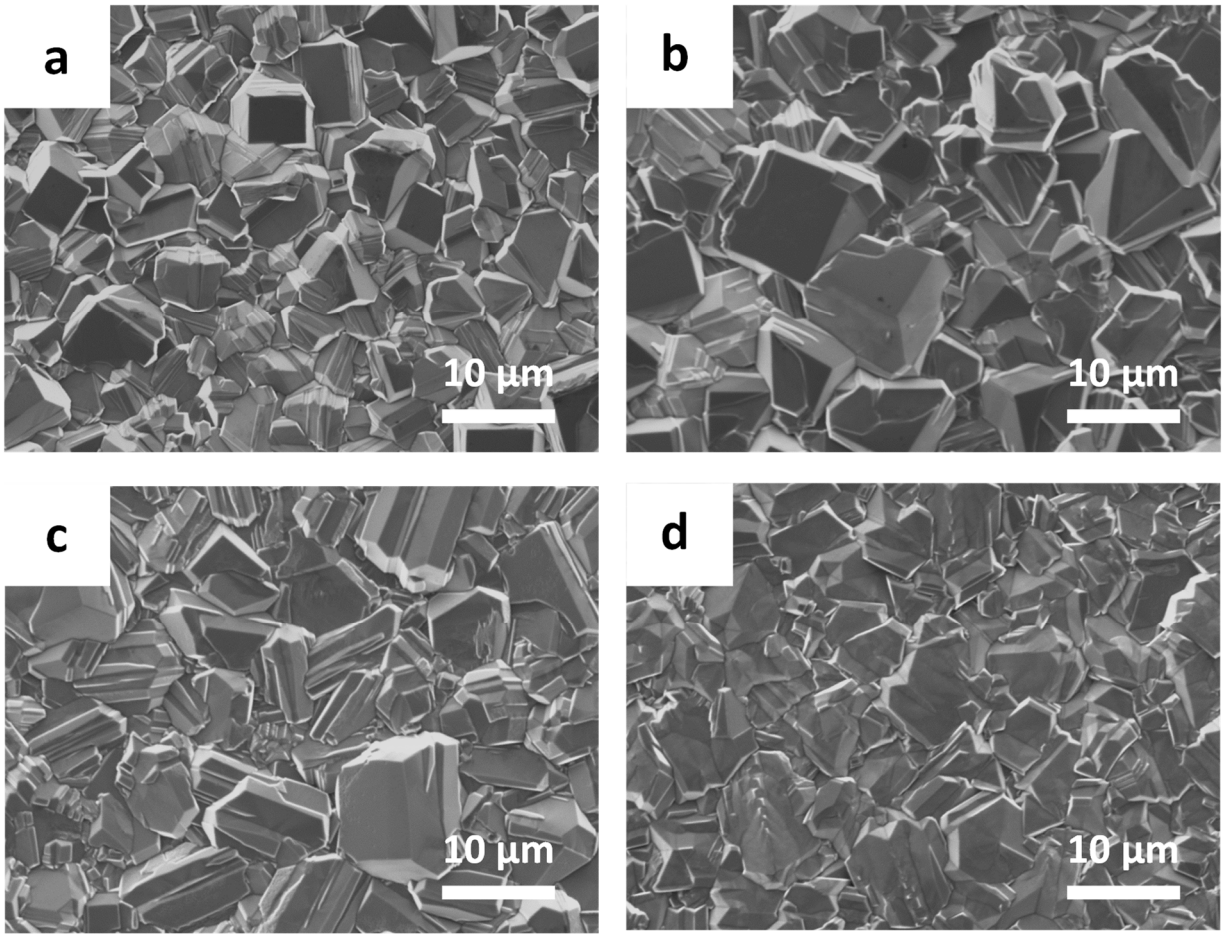

Figure S1. SEM images of BDD electrodes with boron concentration of 0.1% (a), 0.2% (b), 0.5% (c), 1% (d).

When the boron concentration in BDD is relatively low, a sharp peak around 1330 cm^{-1} originating from the sp^3 carbon was observed. On the other hand, as the boron concentration increased, the broad peaks at 500 cm^{-1} and 1200 cm^{-1}, which are due to the vibrational mode of the boron pair and the distortion of the diamond lattice, respectively, were observed to increase. On the other hand, the absence of a peak at 1500 cm^{-1} confirms that the BDD does not contain a significant amount of sp^2 carbon.

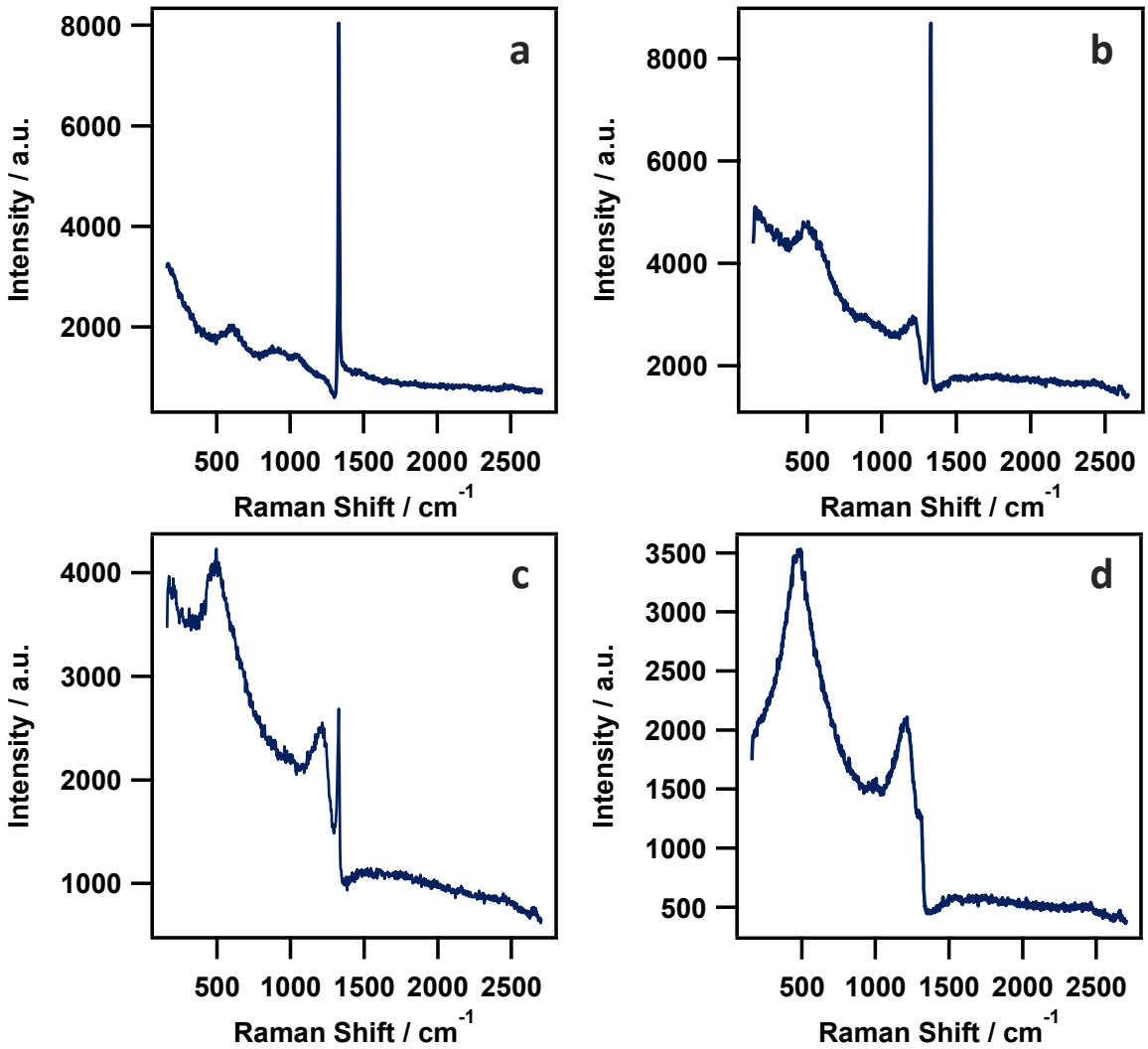

Figure S2. Raman spectra of BDD electrodes with boron concentration of 0.1% (a), 0.2% (b), 0.5% (c), 1% (d).

3. Electrochemical setup

Working electrode geometrical area was 12.56 cm^2 (batch cell) and 9.616 cm^2 (flow cell) delimited by a fluoroplastics O-ring. Counter electrode was a Pt plate of 12.56 cm^2, reference electrode was an Ag/AgCl, sat. KCl (BAS Inc., Japan). Divided batch and flow cell had separated anode and cathode chambers by Nafion membrane (Nafion NRE-212) 0.002 inch thick (3.14 cm^2). The Nafion membrane was conditioned in deionized water for 1 day before use, and stored in a closed vial with deionized water between each experiment. After experiments and before storage, the membrane was placed in deionized water for 1 h. The volume of undivided batch cell is 50 mL and that of divided batch cell and divided flow cell are 50 mL / 50 mL (anolyte / catholyte). N_2 was bubbled at a flow rate of 50 mL min^{-1} for 20 min which was reduced to 20 mL min^{-1} during potentiostatic reduction to remove oxygen that can be reduced during nitrate reduction. The solution was stirred by a Teflon rod made of PTFE, a rotating motor (417-9655, RS components), and a DC stabilized power supply (AD-8724D, A&D Company, Japan).

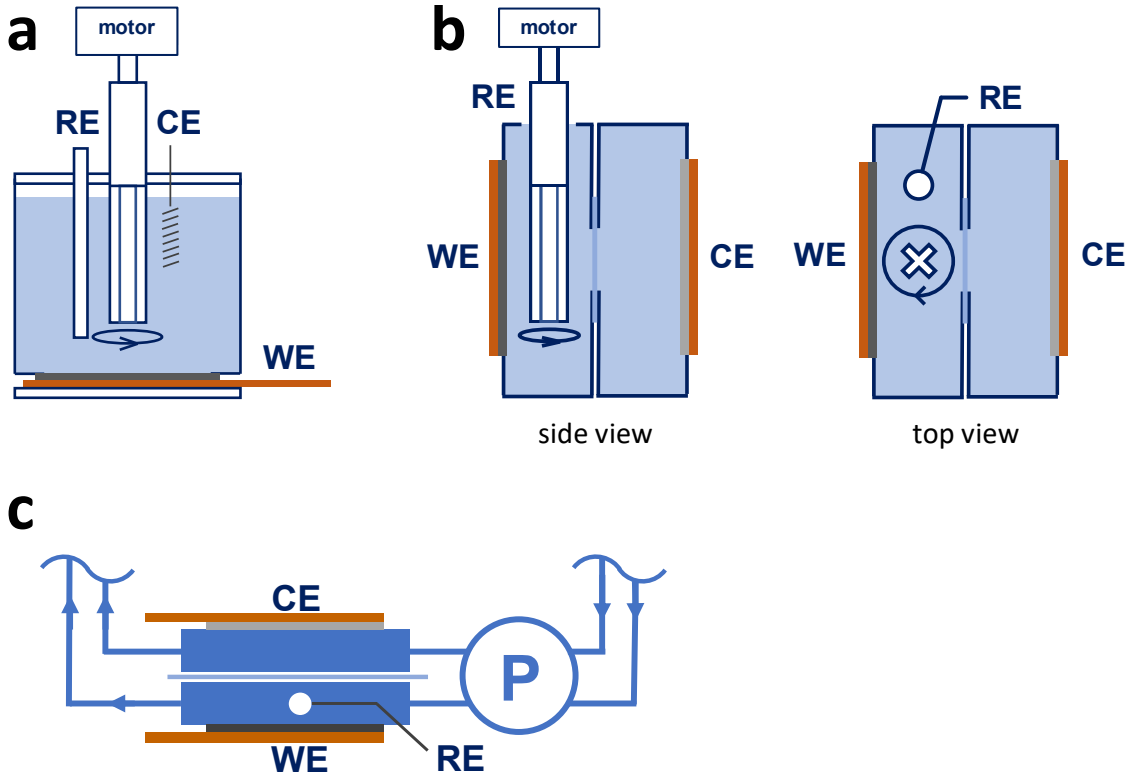

Figure S3. Cell schematic illustrations of undivided batch cell (a), divided batch cell (b) and divided flow cell (c). WE: working electrode; CE: counter electrode; RE: reference electrode; P: peristaltic pump. Copper plate (orange) is used for electrical connections.

4. Products analysis

4.1. NH_3 quantification

Indophenol blue absorbance spectrophotometry with salicylic acid was used for the determination of NH_3. To 2 mL of the diluted electrolyte, 2 mL 1 M NaOH + 5% salicylic acid + 5% trisodium citrate solution, 1 mL 0.05 M NaOCl solution, and 0.2 mL 1wt% $Na_2Fe(CN)_5NO•2H_2O$ solution were added in that order and well stirred. After 30 minutes at room temperature, NH_3 was determined by measuring the absorbance at 655 nm by using a UV-visible absorbance spectrophotometer (V-570 UV-Visible/NIR spectrophotometers, JASCO, Japan). A calibration line was prepared by measuring the absorbance of NH_4Cl solution in ultrapure water at various concentrations (Figure S4). The lowest amount of ammonia measured was 2.4 µM (from Figure 2, at -1.2 V) still in not optimized conditions, but already higher than the limit of detection of 1.6 µM.

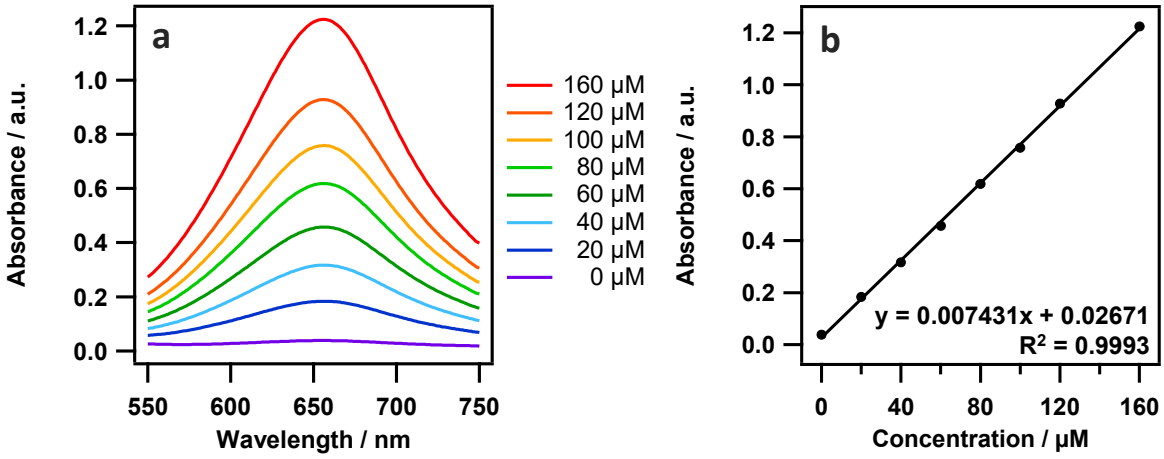

Figure S4. UV-vis absorbance of different concentration of NH_3 (a) and NH_3 calibration line (b). LOD: 1.6 µM.

4.2. NO_2^- quantification

The color reagent was prepared by dissolving 0.2 g of *N*-(1-Naphthyl)ethylenediamine dihydrochloride, 4 g of 4-Aminobenzenesulfonamide (Sulfanilamide), 10 mL of phosphoric acid (85.0wt.%, ρ = 1.685 g mL^{-1}) in 50 mL ultrapure water. After diluting the electrolyte to a quantifiable concentration after reduction by using ultrapure water, 0.1 mL of the color reagent was added to 5 mL of the diluted electrolyte, stirred well, and left at room temperature for 20 min. NO_2^- was determined by measuring the absorbance at 540 nm. Calibration line was prepared by measuring the absorbance of each concentration of $NaNO_2$ in ultrapure water (Figure S5).

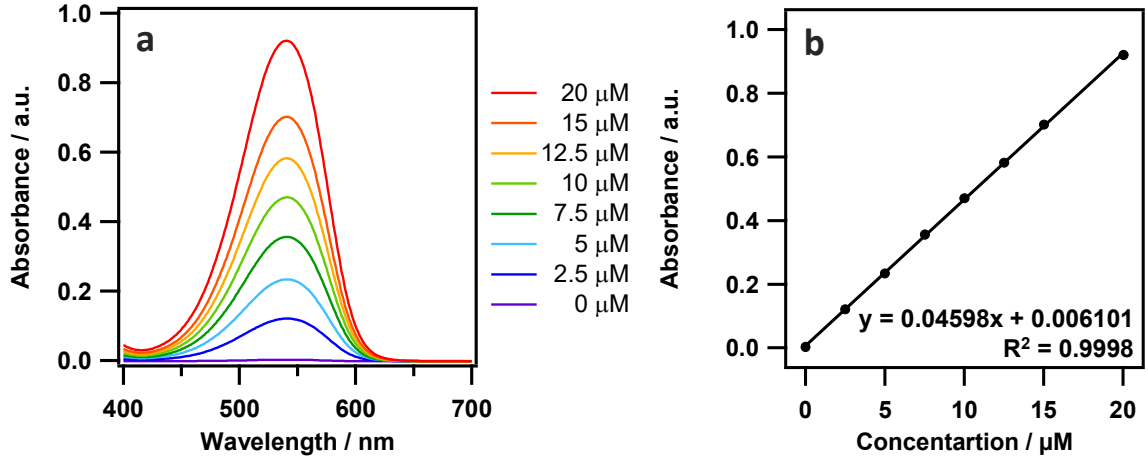

Figure S5. UV-vis absorbance of different concentration of NO_2^- (a) and NO_2^- concentration calibration line (b).

4.3. NO_3^- quantification

After diluting the electrolyte to a quantifiable concentration using ultrapure water, 1 mL of 1 M HCl and 0.1 mL of 0.8 wt% sulfamic acid were added to 4 mL of the diluted electrolyte, stirred well, and NO_3^- determined by measuring the calculated absorbance ($A=A_{220nm}-2A_{275nm}$). A calibration line was prepared by measuring the absorbance of each concentration of $NaNO_3$ in ultrapure water (Figure S6).

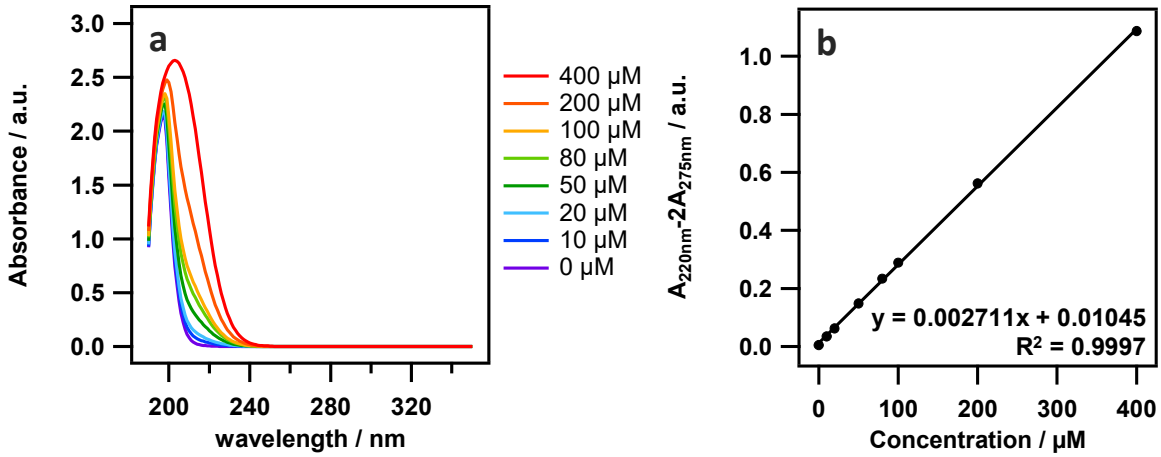

Figure S6. UV-vis absorbance of different concentration of NO_3^- (a) and NO_3^- concentration calibration line (b).

5. Production rate and faradaic efficiency

The production rate is P [μmol cm^{-2} h^{-1}]. It has been calculated (eq S1) from the concentration of each reagent and product c_i [μmol L^{-1}] measured by using the calibration line, the volume of the electrolyte V [L], the geometric area of the electrode S [cm^2], and the electrolysis time t [h], as follows:

$$P = \frac{c_i V}{St} \quad \text{(S1)}$$

From the Faraday law of electrolysis (eq S2), the faradaic efficiency (FE) has been evaluated by eq S3 where n is the number of electrons required for reduction, F [96485 C mol^{-1}] is the Faraday constant, Q [C] is the total charge used in the electrolysis with a current I(t) for a reduction time of T [h] (eq S4).

It is worth noting that the number of electrons required for the reduction of nitrate to ammonia is 8, and the number of electrons required for the reduction of nitrate to nitrite is 2.

$$Q = n \times F \times c \times V \quad \text{(S2)}$$

$$\text{FE} = \frac{n \times F \times c \times V}{Q} \times 100 \quad \text{(S3)}$$

$$Q = \int_0^T I(t)\mathrm{d}t \quad \text{(S4)}$$

6. Optimal B/C ratio of BDD electrodes

Table S1. Current density from linear sweep voltammetry of 0.1 M NaCl (pH 5.9) and 0.1 M $NaNO_3$ (pH 5.8) sampled at –1.8 V vs. Ag/AgCl as function of boron concentration in BDD electrodes.

	B/C %			
	0.1	0.2	0.5	1
$j\ (\mathrm{NaCl})$ / mA cm^{-2}	0.133	0.188	0.306	0.737
$j\ (\mathrm{NaNO_3})$ / mA cm^{-2}	0.661	2.13	2.62	3.07
$\frac{j(\mathrm{NaNO_3}) - j(\mathrm{NaCl})}{j(\mathrm{NaNO_3})} \times 100$	80	91	88	76

In the linear sweep voltammetry measurement of 0.1 M $NaNO_3$, the hydrogen generation reaction compared to the reduction current density of 0.1 M NaCl is not necessarily progressing at the same rate, so this comparison might not be truly accurate, but it is a fair estimate. For this reason, nitrate reduction has been conducted also with 1 % BDD that possesses a higher current density for comparing ammonia production rates (see following results).

7. Potential of electrochemical nitrate reduction

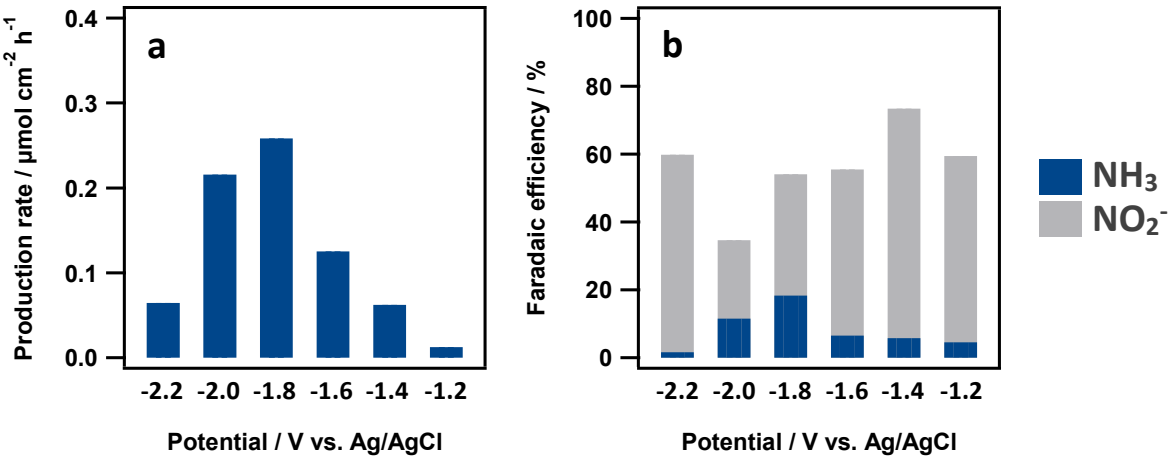

Figure S7. Production rate (a) and faradaic efficiency (b) of electrochemical nitrate reduction using 0.1 M $NaNO_3$ as function of applied potential *vs*. Ag/AgCl (KCl saturated). Results were obtained by using 0.2% BDD as working electrode, electrolysis in divided flow cell, flow rate 200 mL min^{-1}, and 1-hour potentiostatic reduction.

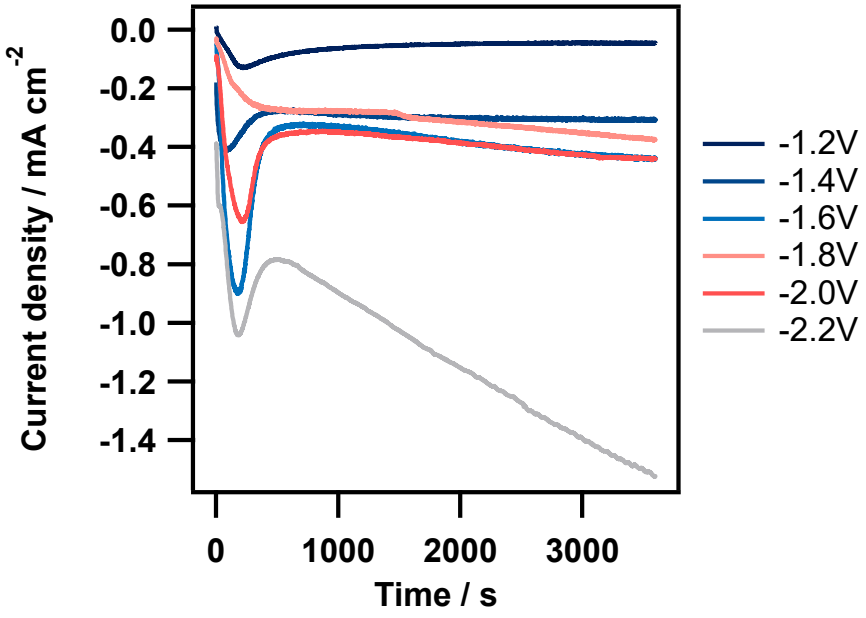

Figure S8. Current density of electrochemical nitrate reduction using 0.1 M $NaNO_3$ as function of applied potential vs. Ag/AgCl (KCl saturated). Results were obtained by using 0.2% BDD as working electrode, electrolysis in divided flow cell, flow rate 200 mL min-1, and 1-hour potentiostatic reduction.

8. Cell types

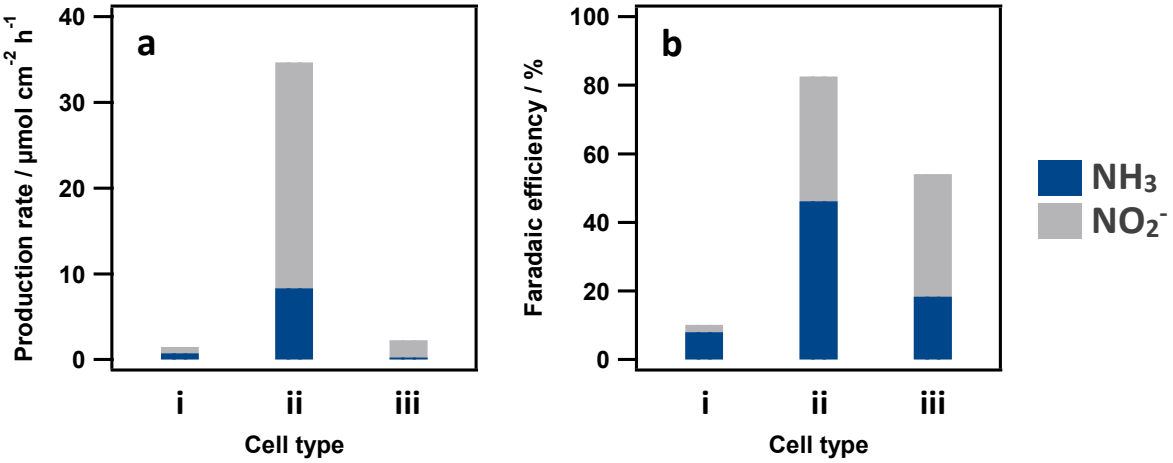

Figure S9. Production rate (a) and faradaic efficiency (b) of: (i) undivided batch cell, (ii) divided batch cell and (iii) divided flow cell. WE: 0.2% BDD. Stirring rate of undivided batch cell and divided batch cell was 2912 rpm and flow rate of divided flow cell was 200 mL min^{-1}. Potentiostatic reduction of 0.1 M $NaNO_3$ at -1.8 V *vs*. Ag/AgCl (KCl saturated) for 1 hour.

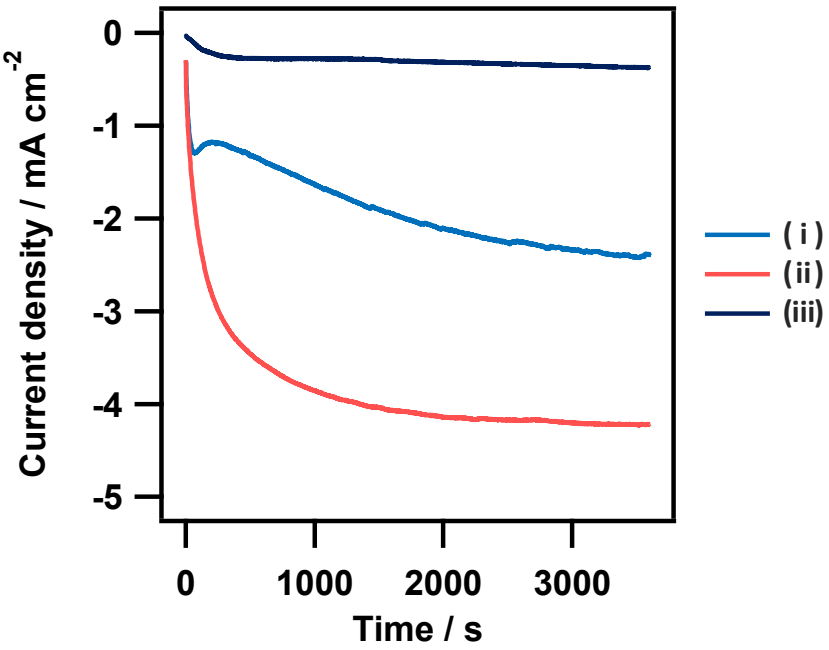

Figure S10. Current density with cell types: (i) undivided batch cell, (ii) divided batch cell and (iii) divided flow cell for the results in Figure S9.

9. Stirring conditions

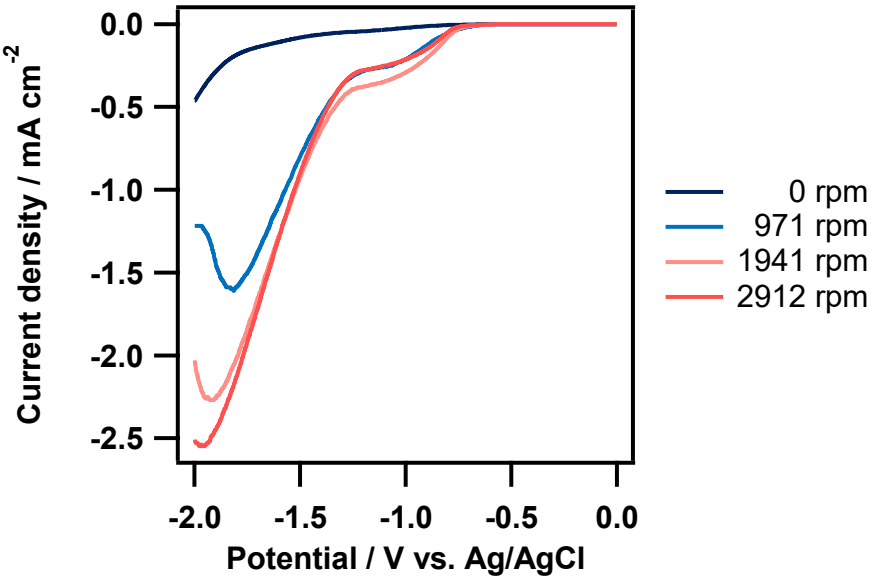

Figure S11. Liner sweep voltammograms (10 mV s^{-1}) of 0.1 M $NaNO_3$ with different stirring rates. Results were obtained by using 0.2% BDD as working electrode and electrolysis in divided batch cell.

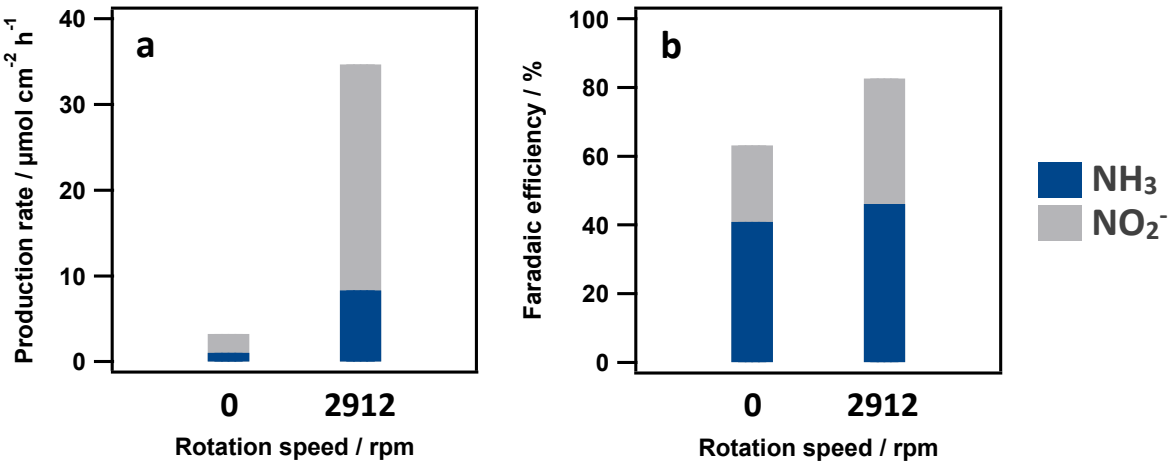

Figure S12. Production rate (a) and faradaic efficiency (b) of electrochemical nitrate reduction using 0.1 M $NaNO_3$ without and with stirring rate at 2912 rpm. Results were obtained by using 0.2% BDD as working electrode, electrolysis in divided batch cell, and 1-hour potentiostatic reduction at -1.8 V *vs*. Ag/AgCl (KCl saturated).

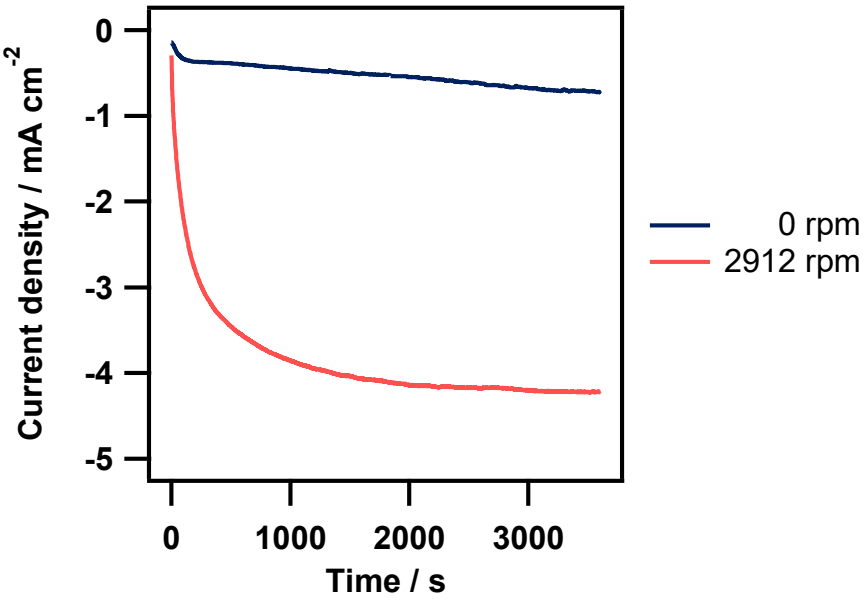

Figure S13. Current density of electrochemical nitrate reduction using 0.1 M $NaNO_3$ without and with stirring rate at 2912 rpm. Results were obtained by using 0.2% BDD as working electrode, electrolysis in divided batch cell, and 1-hour potentiostatic reduction at -1.8 V vs. Ag/AgCl (KCl saturated).

10. Electrolyte pH

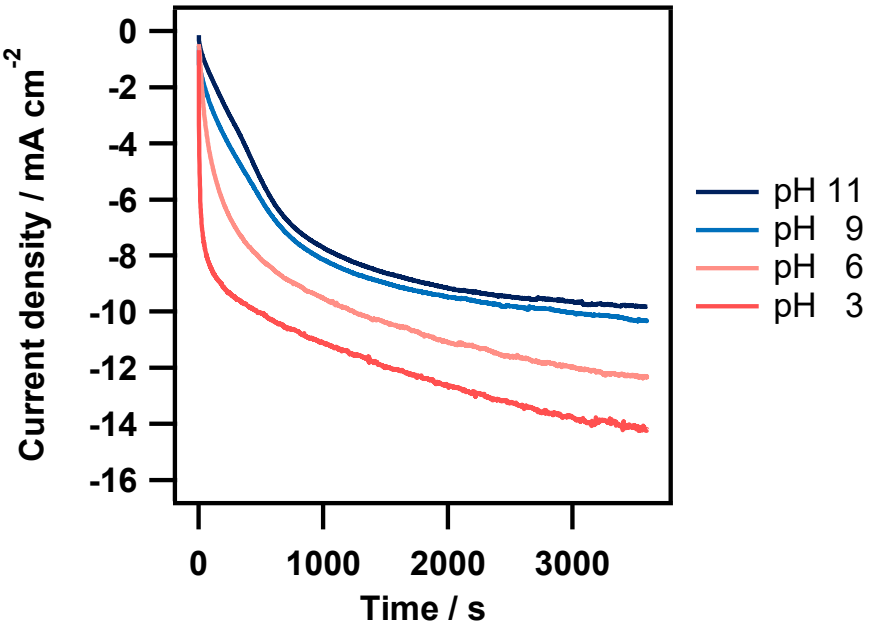

Figure S14. Current density of electrolysis using 0.1 M $NaNO_3$ added with 0.2 M Na_3PO_4 at different pH. Results were obtained by using 0.2% BDD as working electrode, electrolysis in divided batch cell, stirring rate 2912 rpm, potentiostatic reduction at -1.8 V vs. Ag/AgCl (KCl saturated).

11. NaOH concentration

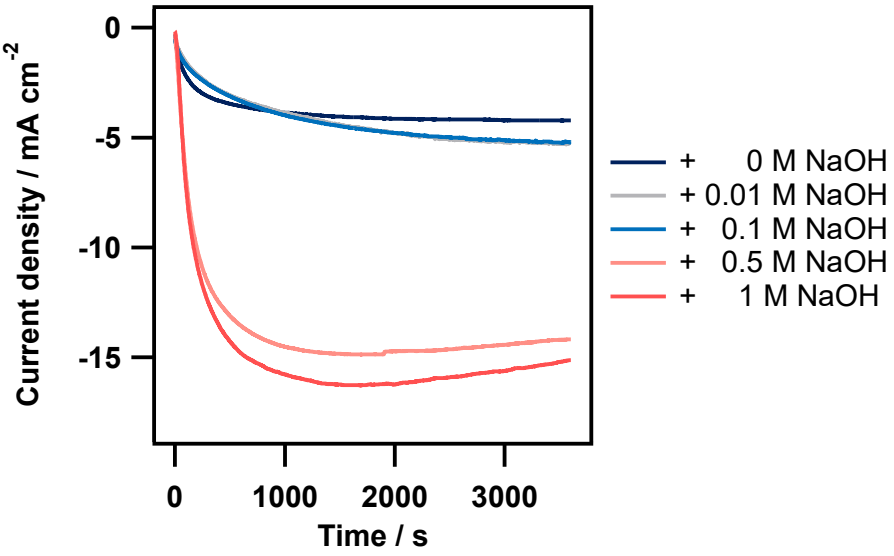

Figure S15. Current density of electrolysis using 0.1 M $NaNO_3$ added with 0, 0.01, 0.1, 0.5, 1 M NaOH. Results were obtained by using 0.2% BDD as working electrode, electrolysis in divided batch cell, stirring rate 2912 rpm, potentiostatic reduction at -1.8 V vs. Ag/AgCl (KCl saturated).

12. Reproducibility of FE_{NH3} and P_{NH3}

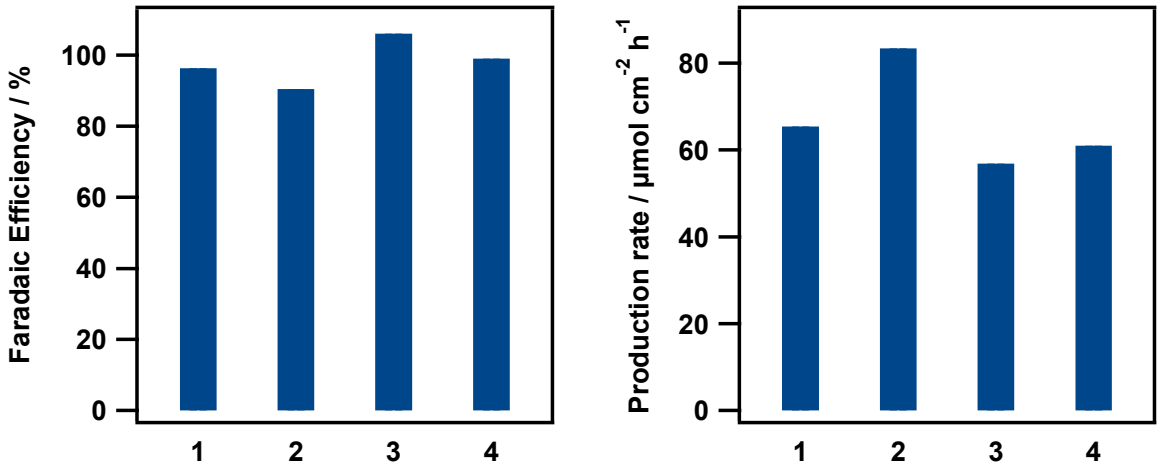

Figure S16. Reproducibility of FE_{NH3} and P_{NH3} for 0.1 M $NaNO_3$ added with 1 M NaOH. WE: 0.2% BDD, divided batch cell, stirring rate 2912 rpm, potentiostatic reduction at –1.8 V *vs*. Ag/AgCl KCl saturated.

13. Electrolyte anion effect

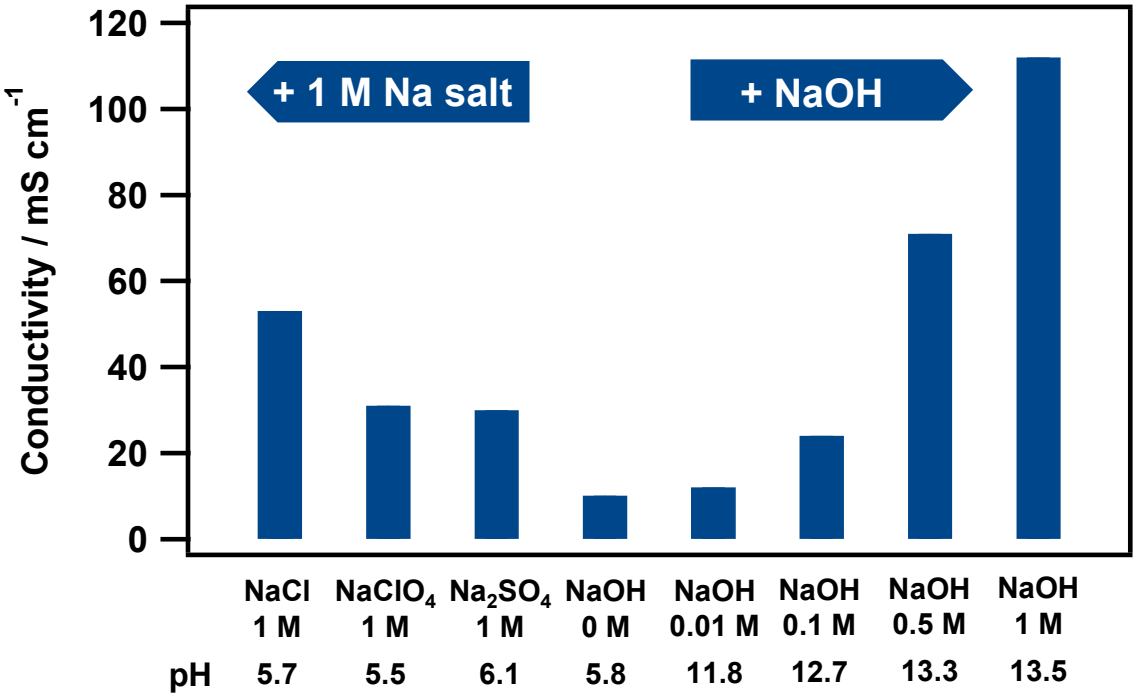

Figure S17. Electrolyte conductivity and pH of solutions used in the nitrate reduction added with different 1M Na salts or NaOH concentrations. All electrolytes contain 0.1 M $NaNO_3$.

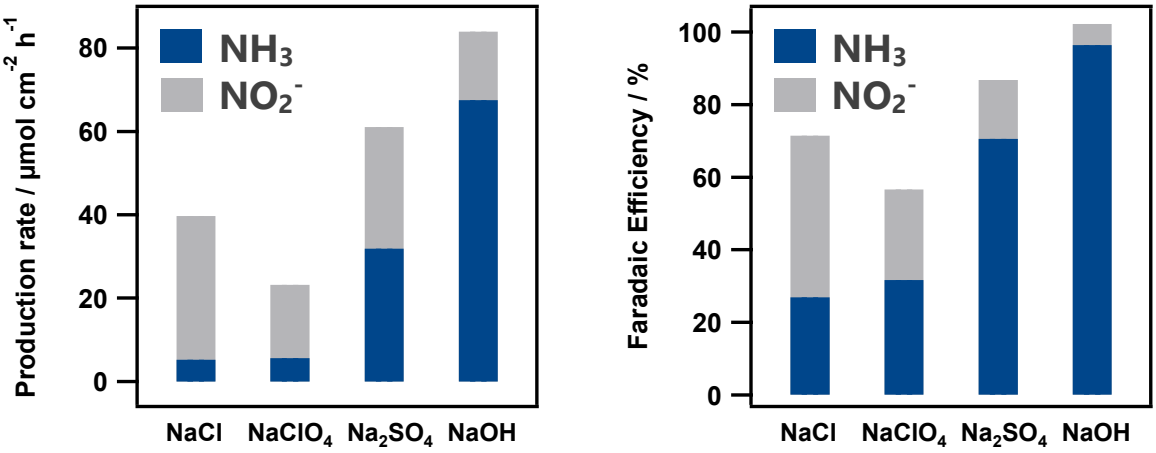

Figure S18. Production rate and faradaic efficiency for the reduction of 0.1 M $NaNO_3$ added with 1 M of the Na salt, respectively. WE: 0.2% BDD. Divided batch cell, stirring rate 2912 rpm, and 1-hour potentiostatic reduction at –1.8 V *vs*. Ag/AgCl (KCl saturated).

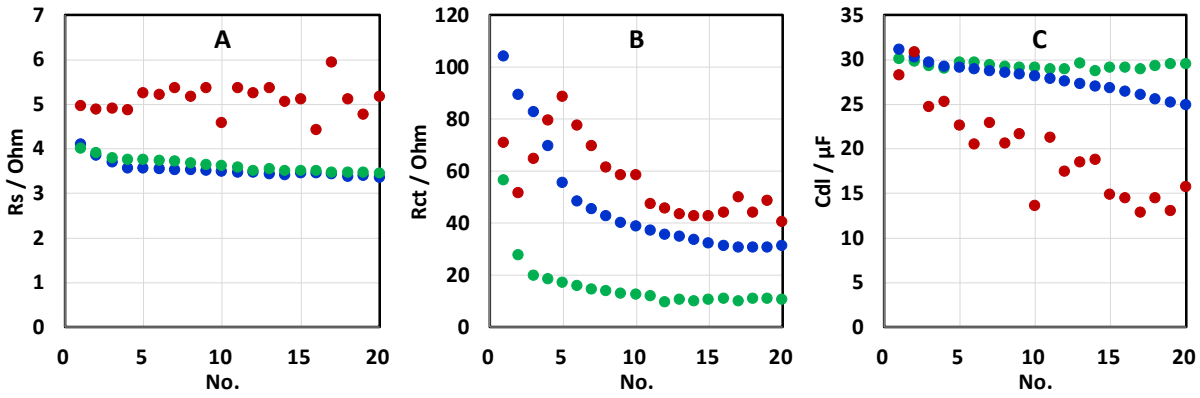

Figure S19. Solution resistance (A), charge transfer resistance (B) and double layer capacitance (Cdl) of 0.1 M $NaNO_3$ added with 1 M salts: NaCl (green), $NaClO_4$ (red), and Na_2SO_4 (blue). Data were measured by EIS at -1.8 V vs. Ag/AgCl (KCl saturated) for 20 consecutive times until steady state. Frequency range: 1 MHz – 10 mHz. Modulation amplitude 10 mV.

14. Linear sweep voltammetry: NaOH concentration effect

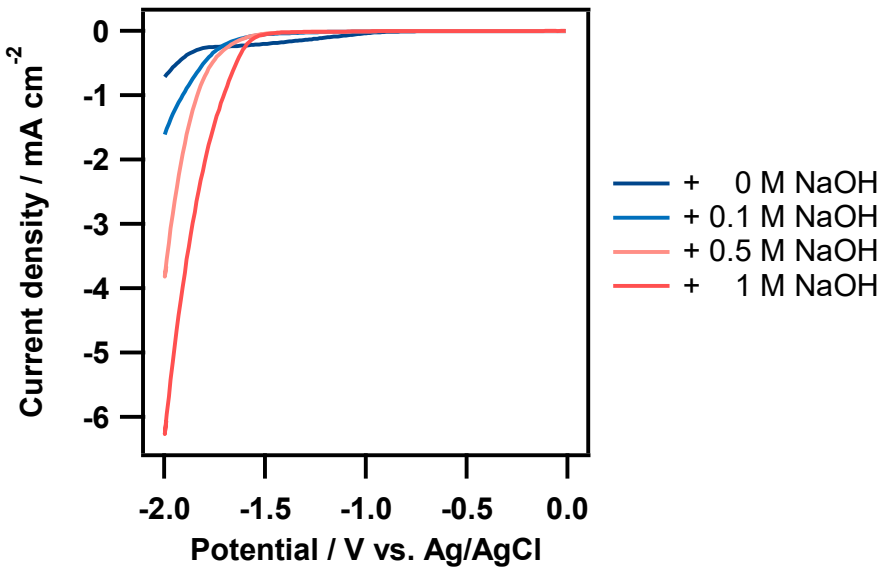

Figure S20. Liner sweep voltammogram at 10 mV s^{-1} of 0.1 M $NaNO_3$ without and with 0.1, 0.5, 1 M NaOH. Results were obtained by using divided batch cell without stirring. V *vs.* Ag/AgCl (KCl saturated).

15. Electrochemical impedance spectroscopy: NaOH concentration effect

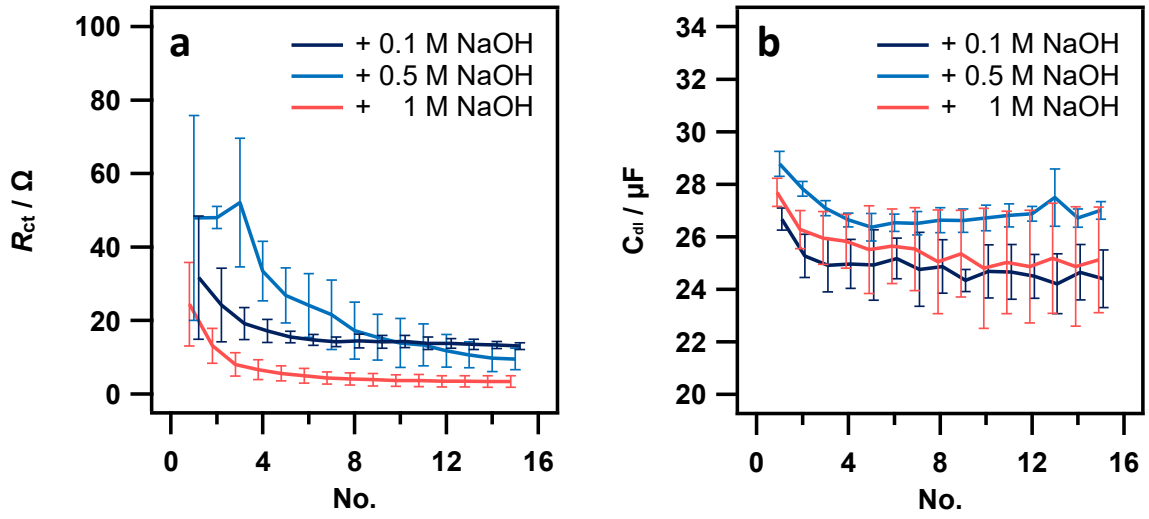

Figure S21. Charge transfer resistance R_{ct} (a) and double layer capacitance C_{dl} (b) of 0.1 M $NaNO_3$ added with 0.1, 0.5, 1 M NaOH. Data were measured by EIS for 15 consecutive times at -1.8 V *vs*. Ag/AgCl (KCl saturated). Frequency range: 1 MHz – 10 mHz. Modulation amplitude 10 mV. Error bar is the standard deviation (n=3).

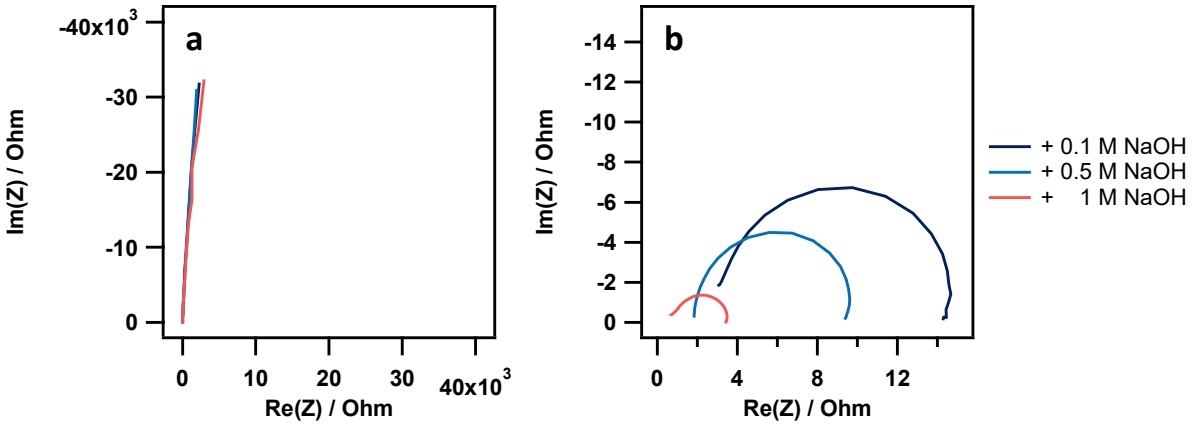

Figure S22. Representative potentiostatic electrochemical impedance spectroscopy measurements at OCP (a) and at -1.8 V *vs* Ag/AgCl (KCl sat.) (b) of 0.1 M $NaNO_3$ added with NaOH. Frequency range: 1 MHz – 10 mHz. Modulation amplitude 10 mV.

16. Time dependence of electrochemical nitrate reduction

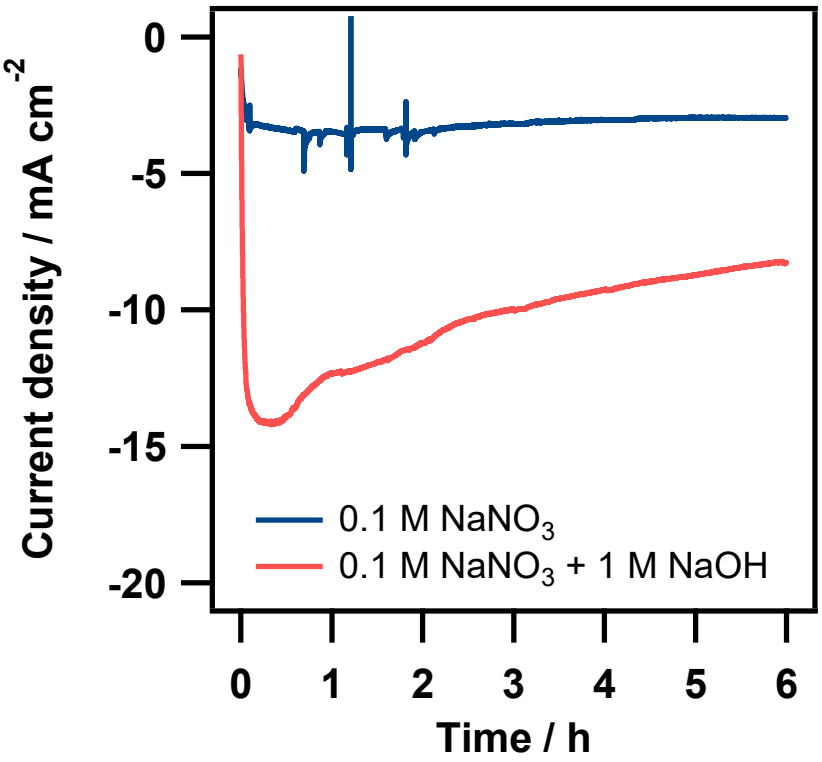

Figure S23. Current density of electrolysis using 0.1 M $NaNO_3$ (blue) and 0.1 M $NaNO_3$ added with 1 M NaOH (red). Results were obtained by using 0.2% BDD as working electrode, electrolysis in divided batch cell, stirring rate 2912 rpm, and 6-hour potentiostatic reduction at -1.8 V *vs*. Ag/AgCl (KCl saturated).

17. Kinetic accounting for NH_3 leaking or other products

Since the present system was tested under strong basic conditions (pH 13.48), it is possible that NH_3 dissolved in the aqueous solution could vaporize into the gas phase. In fact, the smell from the solution in the working electrode chamber after electrolytic reduction gave off an ammonia odor, and because slow N_2 bubbling (to avoid oxygen entering the NaOH electrolyte) and intense stirring were used during the electrochemical nitrate reduction, ammonia could easily escape into the gas phase. We added and ideal term to account for this process (eq S5), where ammonia leaks from the electrolyte solution at rate k_3.

$$\mathrm{NH_3(l)} \xrightarrow{k_3} \mathrm{NH_3(g)} \quad \text{(S5)}$$

NH_3(l) is the ammonia effectively measured in the electrochemical cell, NH_3(g) is the ammonia leaking from the cathodic camber.

Reaction rates are (eqs S6-S7):

$$\frac{\mathrm{d[NH_3(l)]}}{\mathrm{d}t} = k_2[\mathrm{NO_2^-}] - k_3[\mathrm{NH_3(l)}] \quad \text{(S6)}$$

$$\frac{\mathrm{d[NH_3(g)]}}{\mathrm{d}t} = k_3[\mathrm{NH_3(l)}] \quad \text{(S7)}$$

which integrated are (eqs S8-S9):

$$[\mathrm{NH_3(l)}] = [\mathrm{NO_3^-}]_0 \left\{ \frac{k_1 k_2}{(-k_2 + k_3)(-k_1 + k_3)} \mathrm{e}^{-k_3 t} - \frac{k_1 k_2}{(-k_2 + k_3)(-k_1 + k_2)} e^{-k_2 t} + \frac{k_1 k_2}{(-k_1 + k_3)(-k_1 + k_2)} e^{-k_1 t} \right\} \quad \text{(S8)}$$

$$[\mathrm{NH_3(g)}] = [\mathrm{NO_3^-}]_0 \left\{ -\frac{k_1 k_2}{(-k_2 + k_3)(-k_1 + k_3)} \mathrm{e}^{-k_3 t} + \frac{k_1 k_3}{(-k_2 + k_3)(-k_1 + k_2)} e^{-k_2 t} - \frac{k_2 k_3}{(-k_1 + k_3)(-k_1 + k_2)} e^{-k_1 t} + 1 \right\} \quad \text{(S9)}$$

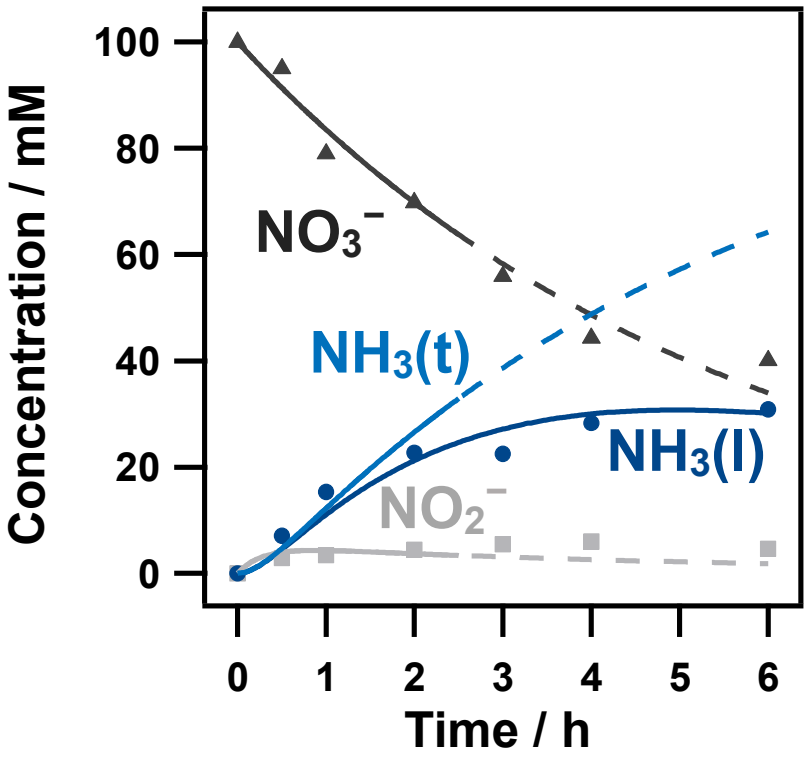

Figure S24. Time dependence of NO_3^-, NO_2^- and NH_3 (dots) and fitting lines of 6 hours electrochemical nitrate reduction using 0.1 M $NaNO_3$ added with 1 M NaOH. Dashed fitting lines are for total (NO_3^-, NO_2^- and NH_3) concentration below 95 mM. NH_3(t) is the theoretical ammonia concentration if leaking was not present.

The reaction constants were $k_1 = 5 \times 10^{-5}$ s^{-1} and $k_2 = 1 \times 10^{-3}$ s^{-1}, the same as from Figure 6 fitting, while for the ammonia leaking into gas phase it was computed as $k_3 = 7 \times 10^{-5}$ s^{-1} (Figure S23).

18. Linear polarization / Tafel slope

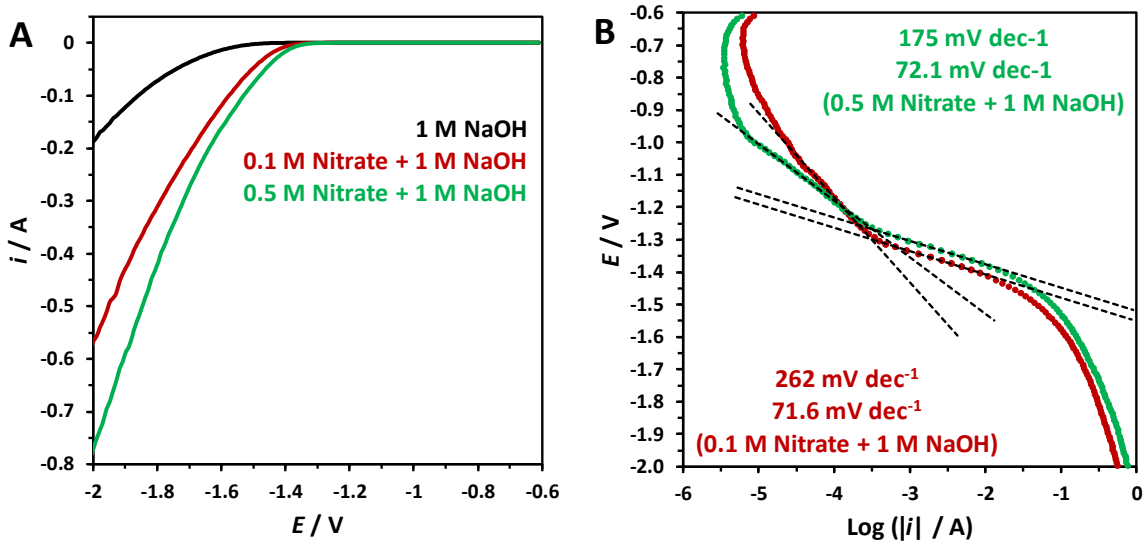

Figure S25. Linear polarization of 1 M NaOH (black), and added with either 0.1 M (red) or 0.5 M (green) $NaNO_3$ (A). Log of reduction current vs *E* to derive the Tafel slope (B). V vs Ag/AgCl, KCl sat. Batch cell with stirring at 2912 rpm, scan rate of 0.0005 V s^{-1}, and step potential of 0.01 V.

19. Comparison of BDD with other electrodes materials

19.1. Copper and titanium

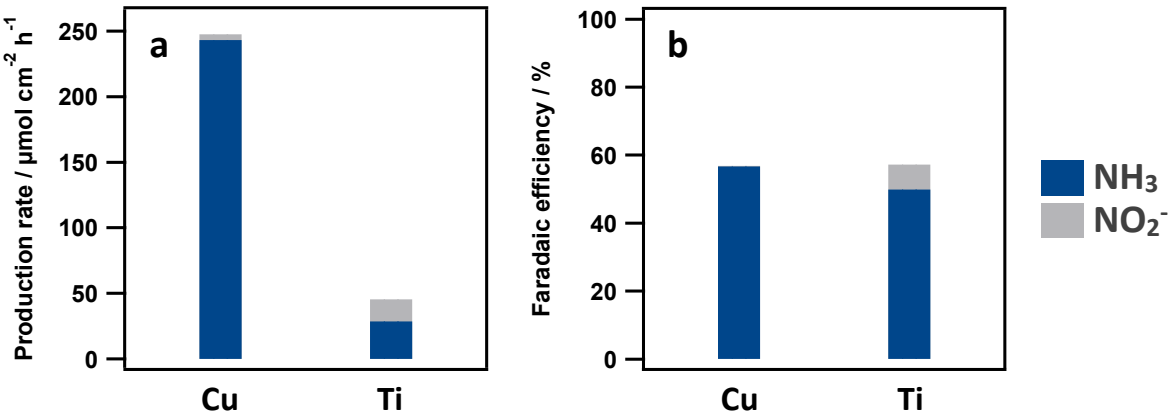

Figure S26. Production rate (a) and faradaic efficiency (b) of electrochemical nitrate reduction using Cu or Ti electrode in divided batch cell with 2912 rpm stirring rate. Cu electrode: 0.1 M $NaNO_3$ with 1 M NaOH, 1-hour potentiostatic reduction at -1.8 V *vs*. Ag/AgCl (KCl sat). Ti electrode: 0.3 M KNO_3 with 0.1 M HNO_3 (pH 1.060), 2 hours potentiostatic reduction at -1.26 V *vs*. Ag/AgCl, KCl sat. (-1 V *vs*. RHE), according to ref. 1.

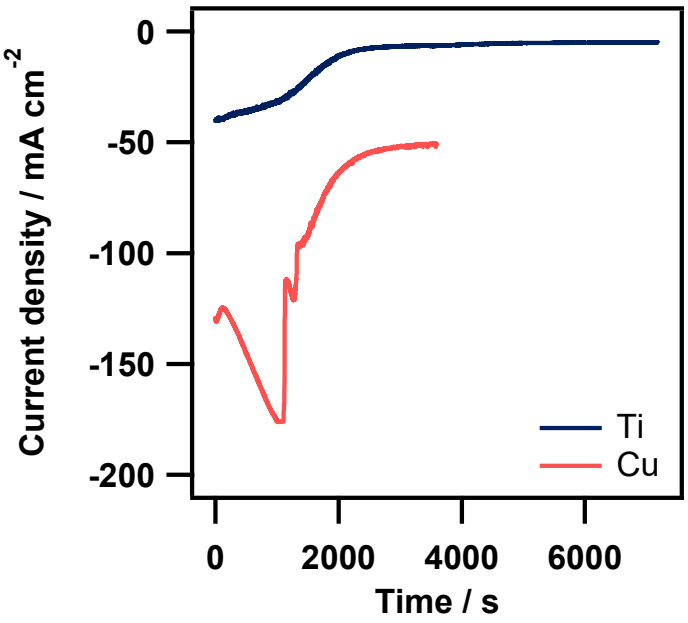

Figure S27. Current density for Cu (red) and Ti (blue) electrodes.

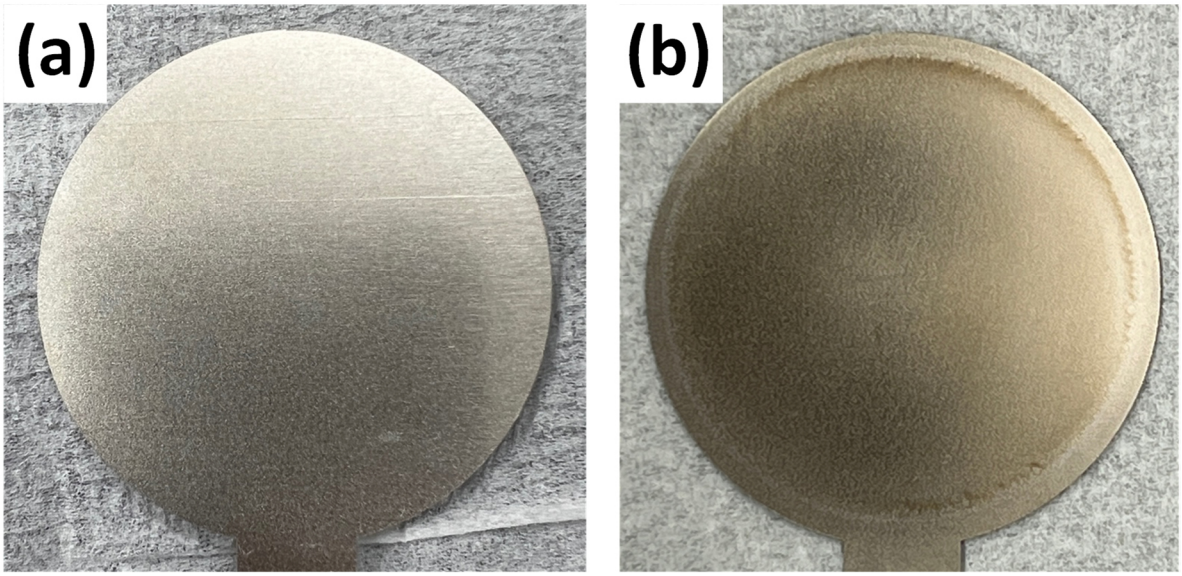

Figure S28. Ti electrode photo image before electrolysis (a) and after electrolysis (b).

19.2. Glassy carbon (GC)

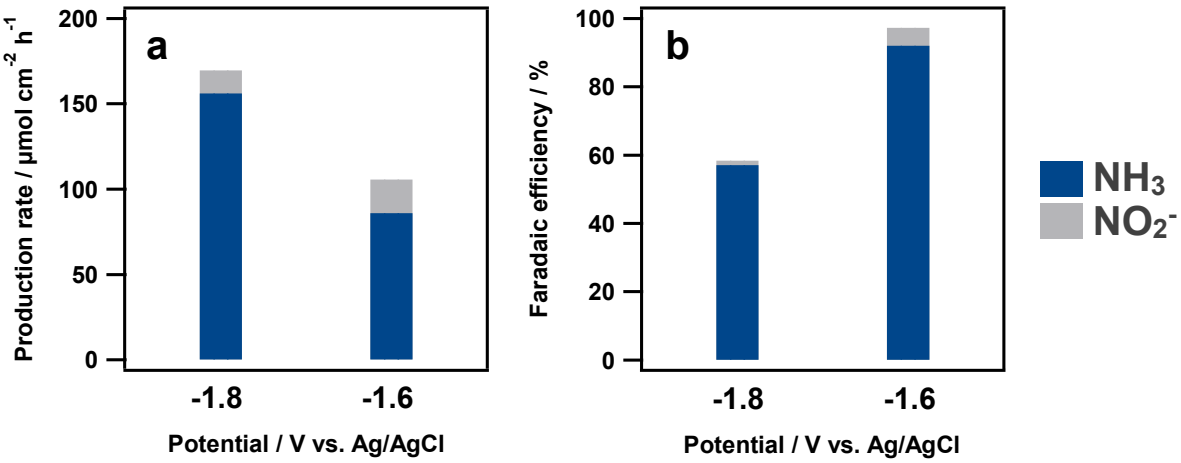

Figure S29. Ammonia production rate (a) and faradaic efficiency (b) of electrochemical nitrate reduction using glassy carbon electrode as working electrode and 0.1 M $NaNO_3$ added with 1 M NaOH. Results were obtained by using divided batch cell, stirring rate 2912 rpm, and 1-hour potentiostatic reduction at -1.6 V and -1.8 V *vs*. Ag/AgCl (KCl saturated).

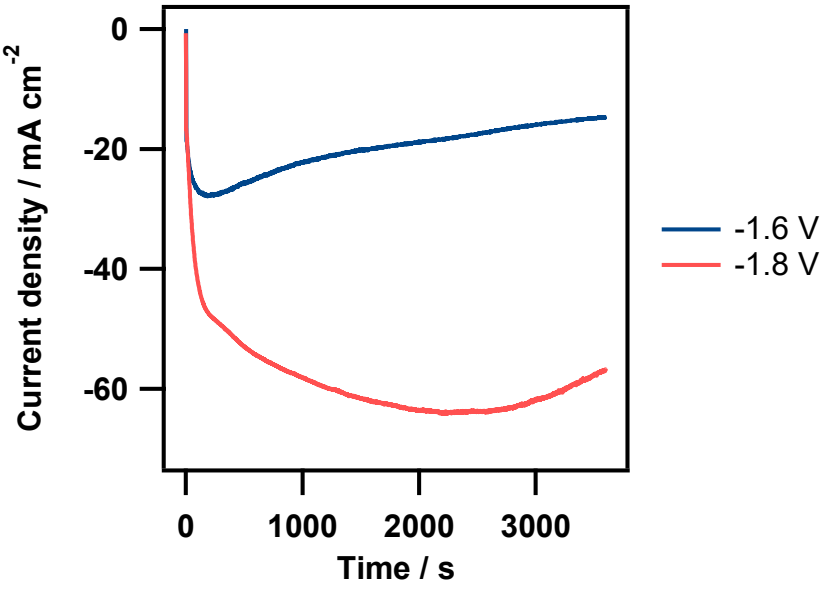

Figure S30. Current density for glassy carbon electrode.

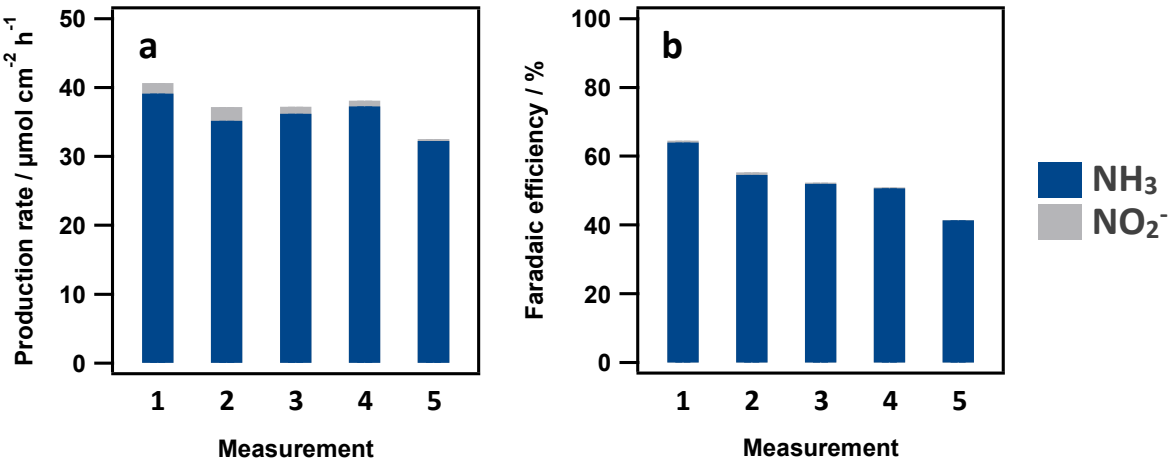

Figure S31. Ammonia production rate (a) and faradaic efficiency (b) of electrochemical nitrate reduction using glassy carbon electrode for 5 consecutive experiments. Electrolyte: 0.1 M $NaNO_3$ with 1 M NaOH. Divided batch cell with stirring rate at 2912 rpm. Potentiostatic reduction at -1.6 V *vs*. Ag/AgCl (KCl saturated) for 6 hours each measurement.

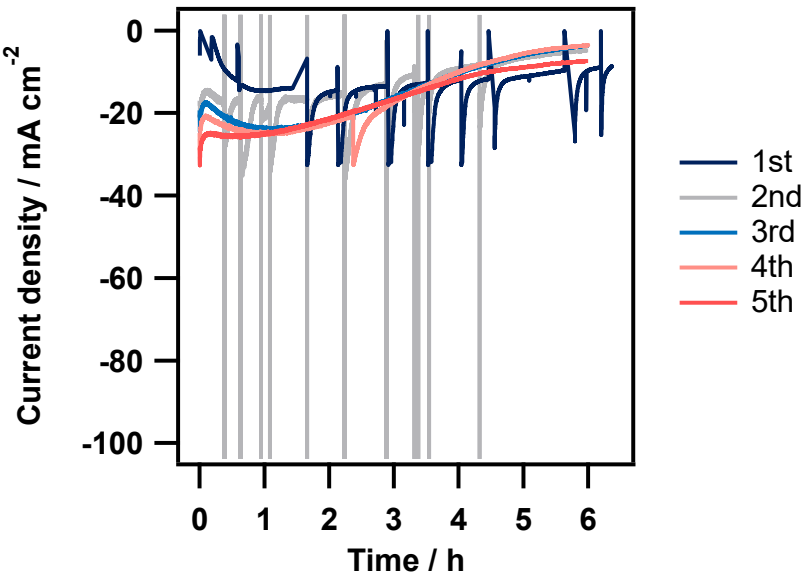

Figure S32. Current density for glassy carbon electrode for 5 consecutive experiments.

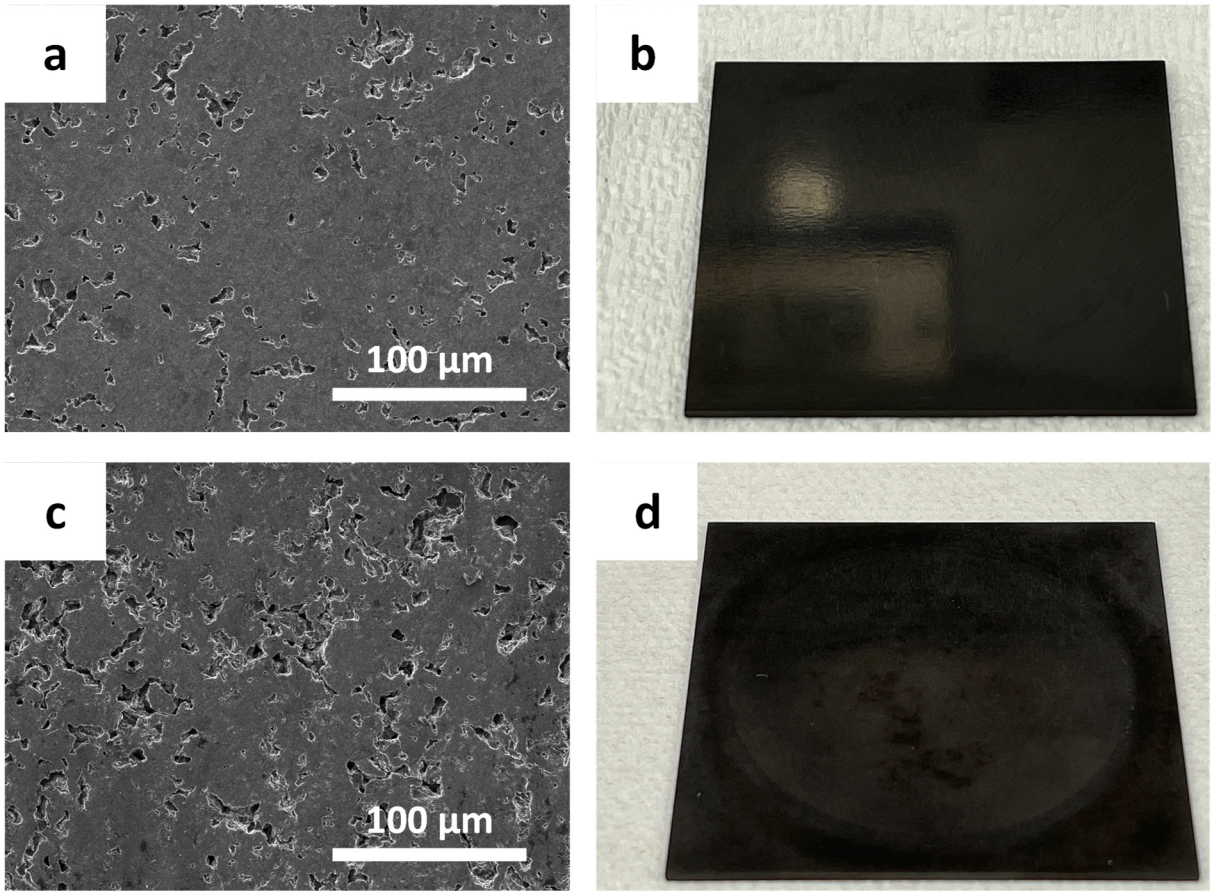

Figure S33. SEM images of glassy carbon electrode before electrolysis (a) and after electrolysis (c), and photo images before electrolysis (b) and after electrolysis (d).

20. Ammonia production stability with BDD

20.1. Production rate and faradaic efficiency

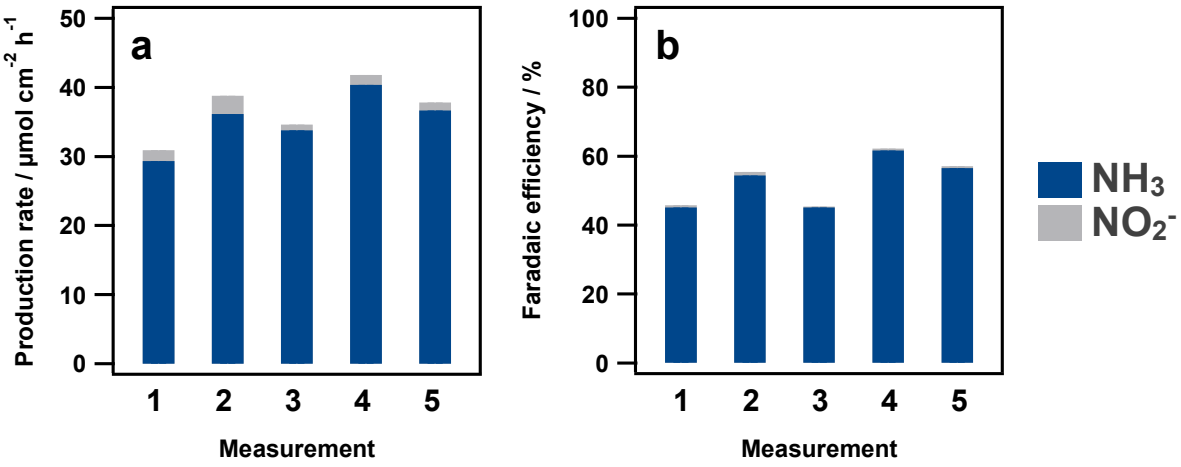

Figure S34. Ammonia production rate (a) and faradaic efficiency (b) of electrochemical nitrate reduction using 0.2% BDD electrode for 5 consecutive experiments. Electrolyte: 0.1 M $NaNO_3$ with 1 M NaOH. Divided batch cell with stirring rate at 2912 rpm. Potentiostatic reduction at -1.8 V *vs*. Ag/AgCl (KCl saturated) for 6 hours each measurement.

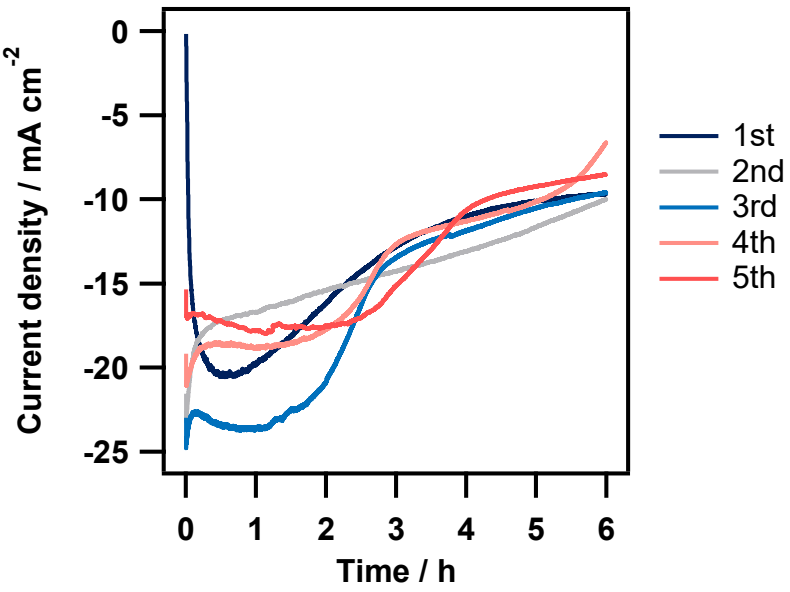

Figure S35. Current density for BDD electrode for 5 consecutive experiments.

20.2. BDD surface investigation after nitrate reduction

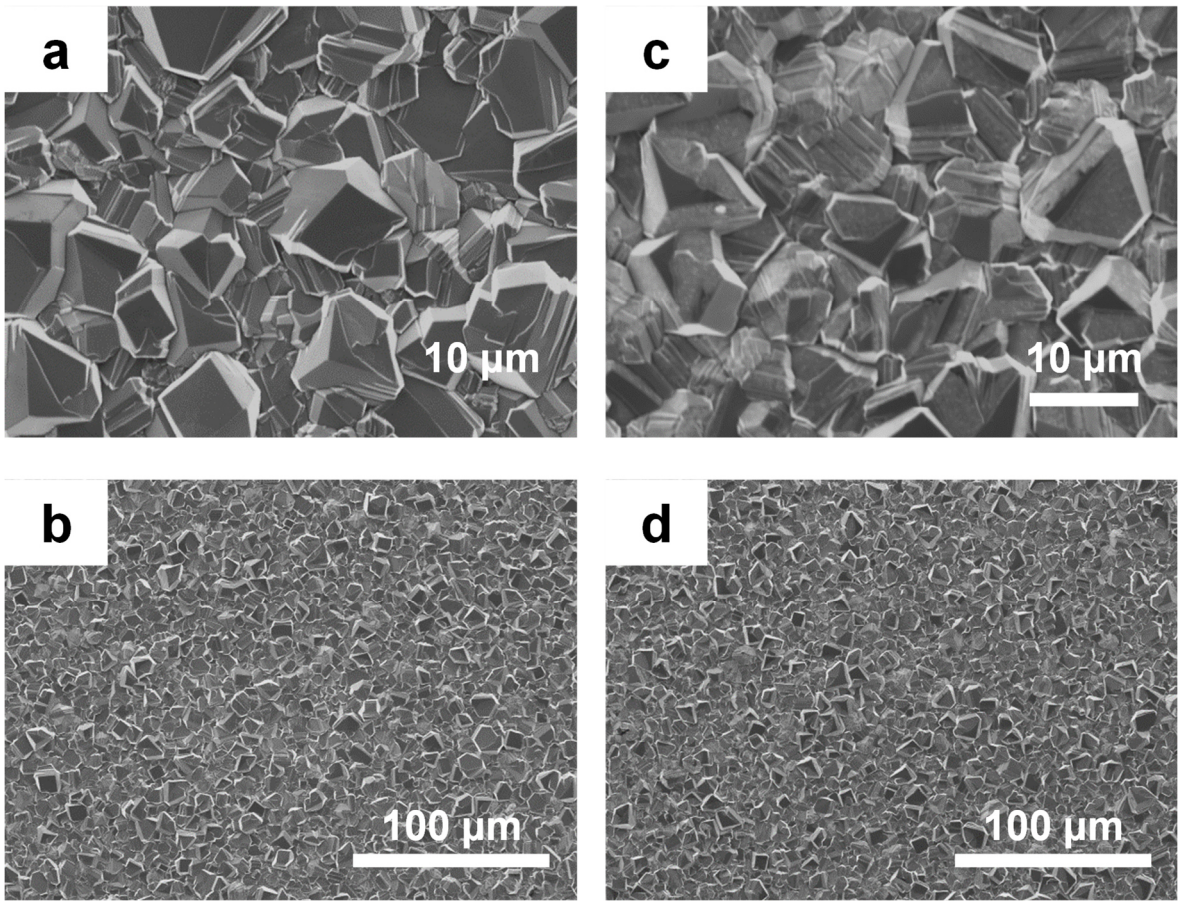

Figure S36. SEM images of the BDD electrode surface before (a,b) and after (c,d) electrochemical nitrate reduction stability test (5 consecutive experiments for 6 hours each).

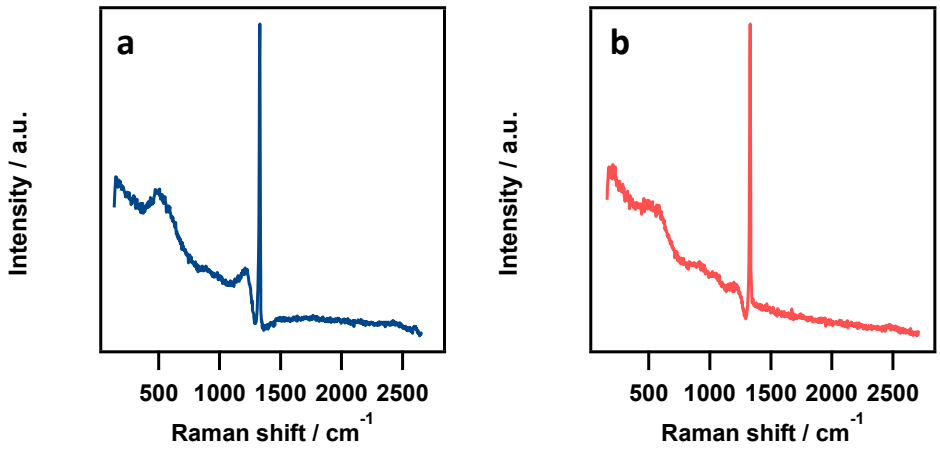

Figure S37. Raman spectra of the BDD electrode surface before (a) and after (b) electrochemical nitrate reduction stability test (5 consecutive experiments for 6 hours each).

21. Increasing ammonia production rate by 1% B/C BDD

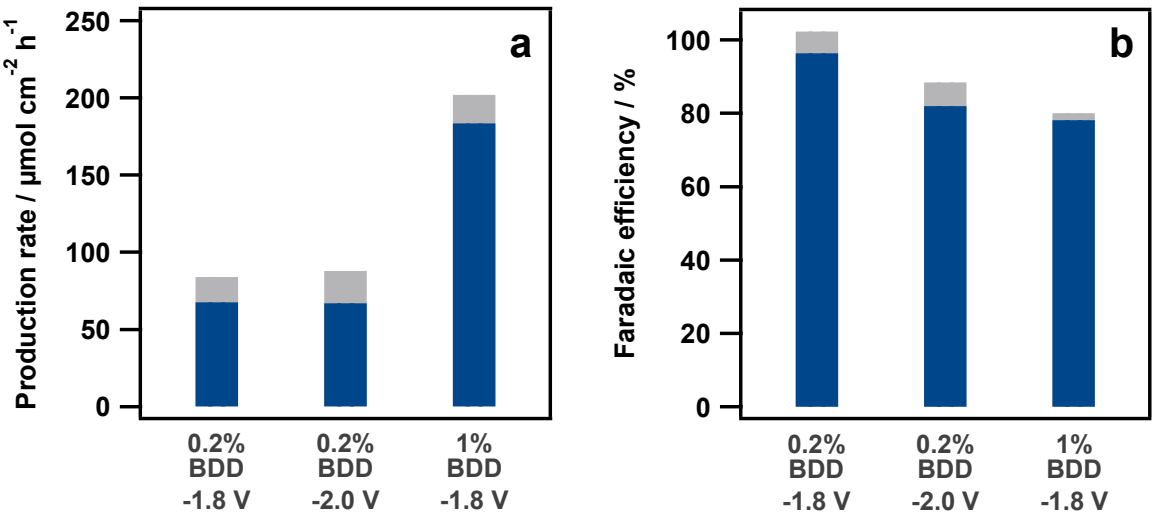

Figure S38. Ammonia production rate (a) and faradaic efficiency (b) of electrochemical nitrate reduction using 0.2% and 1% BDD electrode as working electrode and 0.1 M $NaNO_3$ added with 1 M NaOH. NH_3 (blue) and NO_2^- (gray). Divided batch cell, stirring rate 2912 rpm, and 1-hour potentiostatic reduction at -1.8 V and -2.0 V *vs*. Ag/AgCl KCl saturated.

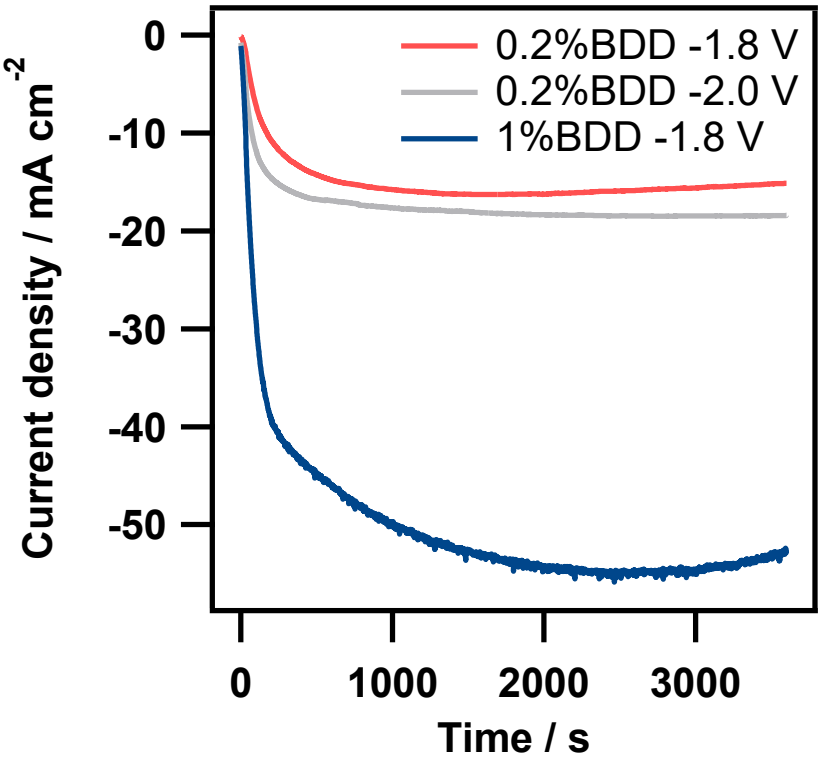

Figure S39. Current density for experiments in Figure S38.

22. Comparison with literature results

Table S2. Comparison of ammonia synthesis by nitrate electrochemical reduction with data available in the literature.

Electrode / catalyst	FE_{NH3} / %	P_{NH3} / μmol cm^{-2} h^{-1}	$[NO_3^-]$ / M	Ref.
Cu	46±11	324±76	1	2
Ag oxide	89	—	0.002	3
Cu(100)	91	34	0.005	4
GaInSn	100	137	0.1	5
Cu/CuOx/Co/CoO	93±2	1170	0.1	6
Pd/TiO_2	92	66	0.25	7
FeB_2	97	1497	0.1	8
C/Co	95.4±1.8	73±1	0.1	9
Zn/CuO	96	55	0.01	10
CoNi	86	4016	0.032	11
$Ni_{85}Rh_{15}$	75	170	0.02	12
CuO	96	245	0.003	13
0.2% BDD	98±6	67±12	0.1	This work
1% BDD	78	184		

23. References

1. McEnaney, J. M.; Blair, S. J.; Nielander, A. C.; Schwalbe, J. A.; Koshy, D. M.; Cargnello, M.; Jaramillo, T. F. Electrolyte Engineering for Efficient Electrochemical Nitrate Reduction to Ammonia on a Titanium Electrode. *ACS Sustainable Chem. Eng.* **2020**, *8* (7), 2672–2681.

2. Barrera, L.; Silcox, R.; Giammalvo, K.; Brower, E., Isip, E.; Chandran, R. B. Combined Effects of Concentration, pH, and Polycrystalline Copper Surfaces on Electrocatalytic Nitrate-to-Ammonia Activity and Selectivity. *ACS Catal.* **2023**, *13* (7), 4178–4192.

3. Liu, H.; Park, J.; Chen, Y.; Qiu, Y.; Cheng, Y.; Srivastava, K.; Gu, S.; Shanks, B. H.; Roling, L. T., Li, W. Electrocatalytic Nitrate Reduction on Oxide-Derived Silver with Tunable Selectivity to Nitrite and Ammonia. *ACS Catal.* **2021**, *11* (14), 8431−8442.

4. Ren, Z.; Shi, K.; Feng, X. Elucidating the Intrinsic Activity and Selectivity of Cu for Nitrate Electroreduction. *ACS Energy Lett.* **2023**, *8* (9), 3658–3665.

5. Crawford, J.; Yin, H.; Du, A.; O'Mullane, A. P. Nitrate-to-Ammonia Conversion at an InSn-Enriched Liquid-Metal Electrode. *Angew. Chem. Int. Ed.* **2022**, *61* (23), e202201604.

6. He, W.; Zhang, J.; Dieckhöfer, S.; Varhade, S.; Brix, A. C.; Lielpetere, A.; Seisel, S.; Junqueira, J. R. C.; Schuhmann, W. Splicing the active phases of copper/cobalt-based catalysts achieves high-rate tandem electroreduction of nitrate to ammonia. *Nat. Commun.* **2022**, *13*, 1129.

7. Guo, Y.; Zhang, R.; Zhang, S., Zhao, Y.; Yang, Q.; Huang, Z.; Dong, B.; Zhi, C. Pd doping-weakened intermediate adsorption to promote electrocatalytic nitrate reduction on TiO2 nanoarrays for ammonia production and energy supply with zinc–nitrate batteries. *Energy Environ. Sci.* **2021**, *14* (7), 3938–3944.

8. Zhang, G.; Li, X.; Chen, K.; Guo, Y.; Ma, D.; Chu, K. Tandem Electrocatalytic Nitrate Reduction to Ammonia on MBenes. *Angew. Chem. Int. Ed.* **2023**, *62* (13), e202300054.

9. Xu S.; Shi, Y.; Wen, Z.; Liu, X.; Zhu, Y.; Liu, G.; Gao, H.; Sun, L.; Li, F. Polystyrene

spheres-templated mesoporous carbonous frameworks implanted with cobalt nanoparticles for highly efficient electrochemical nitrate reduction to ammonia. *Appl. Catal., B* **2023**, *323*, 122192.

10. Du, Z.; Yang, K.; Du, H.; Li, B.; Wang, K.; He, S.; Wang, T.; Ai, W. Facile and Scalable Synthesis of Self-Supported Zn-Doped CuO Nanosheet Arrays for Efficient Nitrate Reduction to Ammonium. *ACS Appl. Mater. Interfaces* **2023**, *15* (4), 5172–5179.

11. Xu, Z.; Wan, L.; Liao, Y.; Pang, M.; Xu, Q.; Wang, P.; Wang, B. Continuous ammonia electrosynthesis using physically interlocked bipolar membrane at 1000 mA cm−2. *Nat. Commun.* **2023**, *14*, 1619.

12. Mattarozzi, L.; Cattarin, S.; Comisso, N.; Musiani, M.; Vázquez-Gómez, L.; Verlato, E. Electrodeposition of Ni−Rh Alloys and their Use as Cathodes for Nitrate Reduction in Alkaline Solutions. *ChemElectroChem* **2023**, *10* (6), e202201122.

13. Wang, Y.; Zhou, W.; Jia, R.; Yu, Y.; Zhang, B. Unveiling the Activity Origin of a Copper-based Electrocatalyst for Selective Nitrate Reduction to Ammonia. *Angew. Chem. Int. Ed.* **2020**, *59* (13), 5350–5354.